Structural, Vibrational, Morphological and Magnetic Properties of Mn-doped $CuFe_2O_4$ Ferrite Nano-Photocatalysts

P. Antony Lyla, E. Thirumal, D. Sahaya Lenin,

Abstract: Unadulterated and Mn-doped CuFe2O4 nano-precious stones were effectively incorporated from its stoichiometric metal nitrates and urea blends, utilizing a microwave helped ignition strategy. Basic and attractive properties have been explored by XRD, FTIR, and VSM examination. Results uncovered that the as-arranged example is a cubic ferrite has high crystallinity. A minor of α-Fe2O3 stage is distinguished, because of inadequacy of response. The normal crystallite size of the as readied Mn-doped CuFe2O4 powders is around 20 to 25nm. FTIR spectra indicated two assimilation groups in the CuFe2O4 structure identified with octahedral and tetrahedral locales in the scope of 400–600 cm-1. The room temperature VSM aftereffects of the examples are speaking to the superparamagnetic conduct of the examples. The immersion polarization estimation of the as readied CuFe2O4 is 29 emu/g was watched and its worth increments to 39 emu/g after Mn-doping. The photocatalytic reactant movement for the as prepared samples was carried out using degradation of methylene blue. The results revealed that the samples are active catalyst.

Keywords: Spinel $CuFe_2O_4$; Microwave method; Nano-photocatalyst; XRD; Methylene blue; VSM.

I. INTRODUCTION

As of late, nanocrystalline spinel ferrites have intrigued novel auxiliary, attractive and electrical properties which regularly vary from these in microstructure scale [1,2]. These properties are appropriate for different applications, for example, segments in recording tape, attractive sensors, biomedical material and attractive reverberation imaging [3,4] and just as being a helpful impetus for synergist oxidation and furthermore corruption of colors [5-10]. Spinel ferrites have the general equation MFe2O4 where M is a divalent particle. The spinel structure depends on a face focused cubic cross section of oxygen particles, shaping tetrahedral (An) and octahedral [B] coordination destinations that might be involved either by M2+ and additionally Fe3+ cations. The present work aims to employ a microwave combustion method to prepare Mn-doped Copper ferrites nanoparticles, and to study the structural and magnetic properties of the samples. It is well known that ferrites are a promising catalyst in large broad of chemical reactions, so that the catalytic activity of Mn-doped $CuFe_2O_4$ nanoparticles will be tested using degradation of MB dye.

Revised Manuscript Received on October 22, 2019.

***** Correspondence Author

P. Antony Lyla *, Department of Physics, Bharath Institute of Higher education and research, Chennai , India

E. Thirumal, Department of Physics, Bharath Institute of Higher Education and Research, Chennai, India

D. Sahaya Lenin, Department of ECE, Bharath Institute of Higher education and research, Chennai , India

The effect of Mn-doping on structural, magnetic and catalytic properties of $CuFe_2O_4$ nanoparticles also was investigated.

II. EXPERIMENTAL PROCEDURES

A. Methods and Materials

Both chemicals have been used as directly from the analytical class obtained from Merck (India). The fuel used was Cu(NO3)2.6H2O, 98%, Fe(NO3)3•9H2O, 98% and CO(NH2)2. With the accumulation of Mn cations of dissimilar molar ratios (MnxCu1-xFe2O4 withx= 0.0, 0.5) to CuFe2O4, the compositions of Mn-doped CuFe2O4 were made. Preparing CuFe2O4 using this technique, the mixtu of the precursor mentioned above.

B. Characterization techniques

The compositions of Mn-doped CuFe2O4 have been made with the aggregation of Mn cations with dissimilar molar ratios (MnxCu1-xFe2O4 with x = 0.0, 0.5) to CuFe2O4.

Photocatalytic corruption of methylene blue was utilized to look at the photocatalytic capability of Mn-doped CuFe2O4 nano-photocatalysts. The UV light was situated at a 5-cm good ways from the arrangement surface. In the wake of including the unadulterated and Mn-doped CuFe2O4 nano-photocatalysts to a MB arrangement, it was mixed precisely for 20 minutes in obscurity for adsorption balance response. Other UV lights were utilized to illuminate the arrangement, and the reactor substance were blended in a mechanical stirrer. It ought to be noticed that all examinations were done at encompassing temperature. For keeping a steady temperature, we set the reactor in a cooling chamber. During light, the examples were gathered at explicit interims and inspected by HPLC after photocatalyst division by an outer magnet.

III. RESULTS AND DISCUSSION

A. Powder XRD analysis

Fig. 1 gives the X-ray diffraction patterns of the as-prepared pure and Mn-doped $CuFe_2O_4$ ferrite samples using microwave assisted combustion method. All the appeared peaks for the as prepared sample can be assigned to the high crystallinity spinel $CuFe_2O_4$ phase (ICDD card no: 72-1174) as shown in Fig. 1 (sample1). The broadening of X-ray lines of Mn-doped $CuFe_2O_4$ was attributed to decrease the crystallite size [23]. Additional peaks corresponding to a small amount of α-Fe_2O_3 (Hematite) as a second phase were observed due to the incomplete reaction [26]. The absence of the ZnO peaks on XRD traces can be due to the lower intensity of X-ray scattering of ZnO compared to α-Fe_2O_3.

The average crystallite size of pure and Mn-doped $CuFe_2O_4$ ferrite samples was calculated using Debye Scherrer formula is given in Eq. (1):

$$L = \frac{0.89\lambda}{\beta \cos\theta} \qquad \text{----------} \qquad \textbf{(1)}$$

where L is the crystallite size, λ, the X-ray wavelength, θ, the Bragg diffraction angle and β, the full width at half maximum (FWHM). The average crystallite size for both the pure and Mn-doped $CuFe_2O_4$ ferrite samples was found to be 27.43 nm and 22.62 nm, respectively [27].

The lattice parameters values of pure and Mn-doped $CuFe_2O_4$ ferrite samples were calculated using the formula given in Eq. (2):

$$d_{hkl} = \frac{a}{\sqrt{h^2 + k^2 + l^2}}$$

or

$$\sin^2\theta = \frac{\lambda^2}{4a^2}(h^2 + k^2 + l^2) \qquad \text{---- (2)}$$

where θ is the diffraction angle, λ, the incident wavelength (λ = 1.540 Å), h, k, and l are Miller's indices. The calculated lattice parameter values are shown in Table 1.

Table 1. Crystallite size (D), and lattice parameter, (a) values of Mn-doped CuFe2O4

Sl. No.	Samples	Crystallite size (nm)	Lattice parameter (Å)
1.	$CuFe_2O_4$	27.43	8.355
2.	$Mn_{0.5}Cu_{0.5}Fe_2O_4$	22.62	8.364

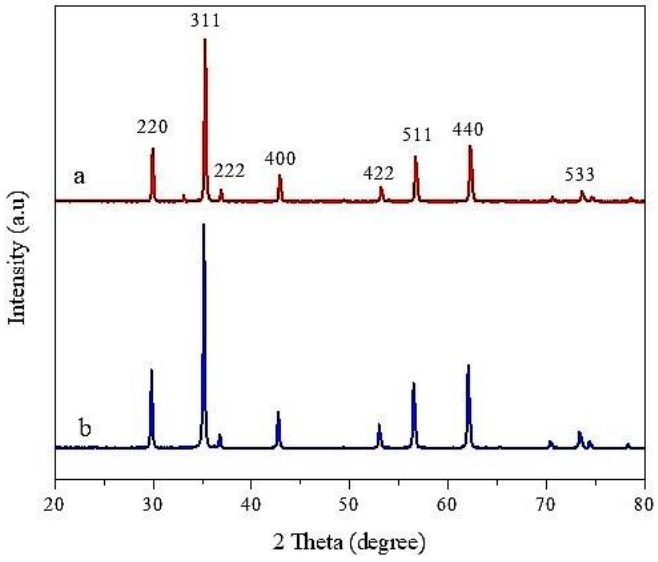

Fig. 1. Powder XRD pattern of pure (a) and Mn-doped $CuFe_2O_4$ NPs (b).

B. Infrared (FT-IR) spectra

FTIR spectra of the as readied unadulterated and Mn-doped CuFe2O4 ferrite tests are appeared in Fig. 2. The spectra show two principle retention groups underneath 1000 cm–1, these two groups are Characteristic groups of the ferrite stage [28]. As indicated by the high recurrence band υ1 and the low recurrence band υ2 is doled out to extending and vibration of tetrahedral and octahedral edifices separately. Contrasts in the estimations of υ1 and υ2 groups are because of various in destinations measurements, where tetrahedral site measurements are little contrasted with the octahedral site measurements [29]. The retention band has a converse association with the bond length. Along these lines, these perceptions demonstrate that nano size unadulterated and Mn-doped CuFe2O4 ferrite tests are rearranged spinel ferrite structure as revealed as of late [30].

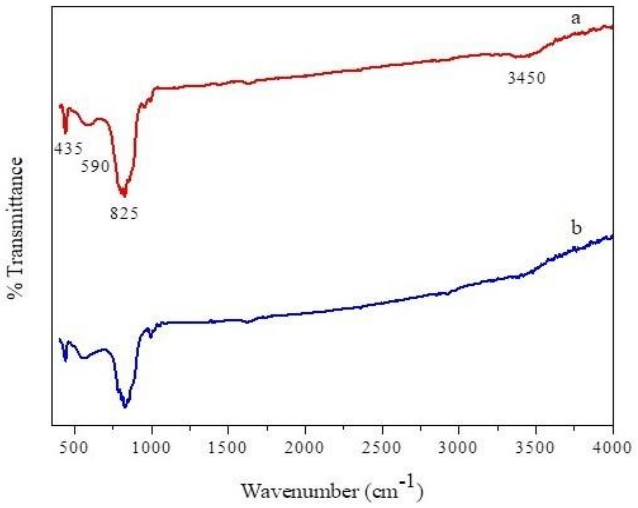

Fig. 2. FT-IR spectra of pure (a) and Mn-doped $CuFe_2O_4$ NPs

C. HR-SEM analysis

HRSEM images of pure and Mn-doped $CuFe_2O_4$ NPs are shown in Figs. 3 represent the formation of spherical-shaped nanoparticles (particle size: ~30 nm). The surface morphologies of these spherical particles in pure and Mn-doped $CuFe_2O_4$ NPs were smooth, uniform, and compact, while the particles were loosely aggregated. The spherical particles had a uniform size distribution.

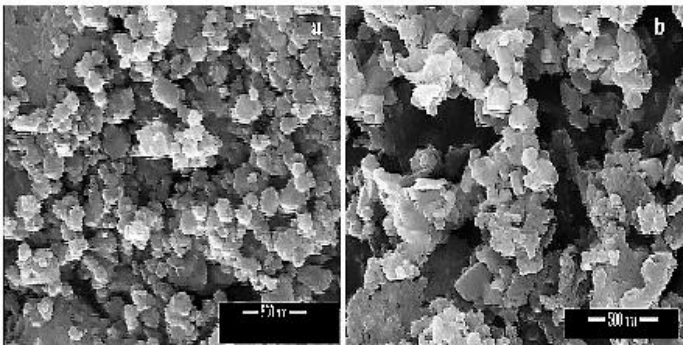

Fig. 3. HR-SEM images of (a) $CuFe_2O_4$ and (b) Mn-doped $CuFe_2O_4$ NPs.

D. EDX analysis

In Figure 4, the elemental composition analytical spectra of $CuFe_2O_4$ NPs are described. The colours depict areas enriched with Fe, Cu, O, in the nanomagnetic photocatalyst. The elements showed a uniform distribution in the nano-magnetic photocatalyst, and identification of Cu, O and Fe confirmed the presence of $CuFe_2O_4$ NPs.

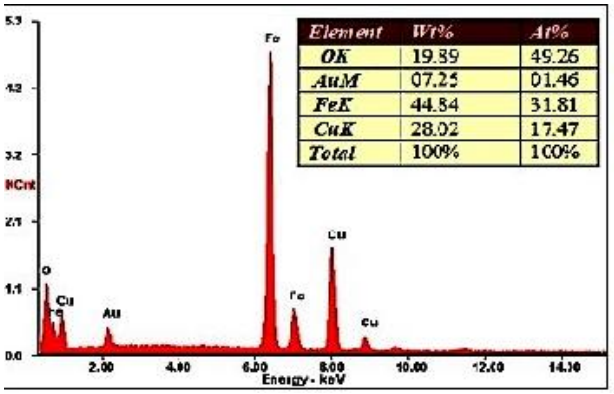

Fig. 4. The EDX spectrum of $CuFe_2O_4$ NPs.

E. HR-TEM analysis

Fig. 5 shows the HR-TEM images and standard electron diffraction (SAED) patterns of pure and Mn-doped CuFe2O4 samples. TEM images show agglomerated particles for both the two samples. Electron diffraction patterns indicate that pure and Mn-doped CuFe2O4 exhibits high crystallinity. The average particle size of the samples observed from TEM images is larger than the estimated values from XRD analysis. This could be attributed to the agglomeration of the particles observed in TEM image due to the high temperature produced while the combustion process.

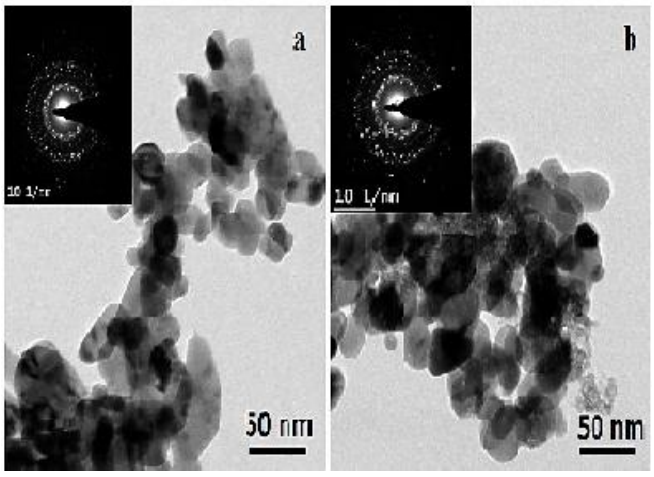

Fig.5. The HR-TEM images of pure (a) and Mn-doped $CuFe_2O_4$ NPs (b).

F. Magnetic properties

A vibrating sample magnetometer (VSM) with an applied magnetic field of 15 kOe was used to test the room temperature magnetization for pure and Mn-doped CuFe2O4 samples. The resulting loops of pure and Mn-doped CuFe2O4 specimens for magnetic hysteresis are shown in Fig. 6. The M-H curves obtained are saturated above 2 kOe and indicate a magnetic order of the samples[31].

Table 2. Magnetic properties (H_c, M_r and M_s) of pure and Mn-doped $CuFe_2O_4$ nano-photocatalysts.

Sl. No.	Samples	H_c (O_e)	M_r (emu/g)	M_s (emu/g)
1.	$CuFe_2O_4$	8.12	0.453	29.55
2.	$Mn_{0.5}Cu_{0.5}Fe_2O_4$	8.65	0.525	39.25

G. Photo-catalytic activity

The photo-catalytic activity of pure and Mn-doped $CuFe_2O_4$ samples was tested for the degradation of MB dye. The obtained results of catalytic performance are given in Table 3 (Figure 7). It is noticed from Table 3 increasing the catalytic activity of the samples with Mn-doped $CuFe_2O_4$ due to increasing specific surface area. It is reported that the active sites on the surface increase with crystallite size decrease [34]. Sample Mn-doped $CuFe_2O_4$ is considered the most active sample when compared to samples pure $CuFe_2O_4$ as it has the larger crystallite size. Also the presence of α-Fe_2O_3 phase enhancement the catalytic performance; where the composition effects on catalytic activity. The present study reveals that the degradation toward MB dye. This behaviour may be attributed to the increase number of active sites on the catalyst surface [35].

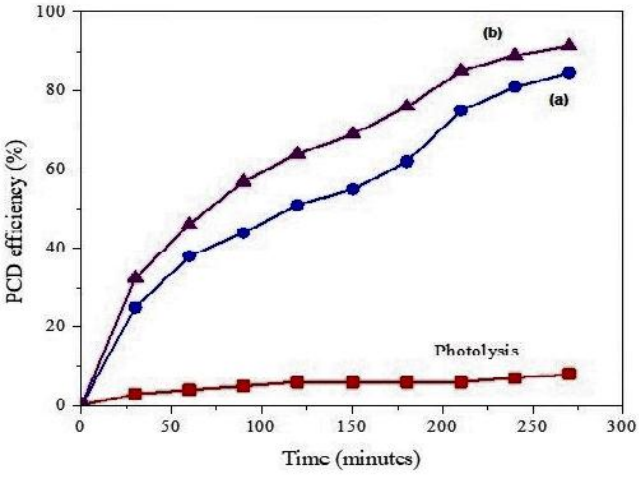

Fig. 7. PCD efficiency of pure (a) and Mn-doped $CuFe_2O_4$ (b) samples

Table 3. PCD percentage for the degradation of MB dye.

SL. No.	Samples	PCD efficiency (%)
1.	$CuFe_2O_4$	84.43
2.	$Mn_{0.5}Cu_{0.5}Fe_2O_4$	95.65

IV. CONCLUSION

Samples of CuFe2O4 pure nanocrystallites and Mn-doped CuFe2O4 were successfully prepared using combustion aided by microwave. Using XRD, FTIR, HR-SEM, HR-TEM and VSM analysis, structural properties of the specimens are investigated. The results showed that samples in the nano-scale with a high purity, the crystallite volume, were spinel-pure and Mn-doped CuFe2O4 structure. The step -Fe2O3 was detected because of incompleteness. Magnetic results were obtained by VSM at room temperature, and it showed that the samples are magnetically ordered. The saturation magnetization and coercive field values increased slightly after Mn-doping. The catalytic performance of the samples was tested using MB dye. The results revealed that the prepared samples are active and towards the degradation of dye.

REFERENCES

1. K. Seevakan, A. Manikandan, P. Devendran, Y. Slimani, A. Baykal, T.Alagesan, Ceramics International, 44 (2018) 20075-20083.
2. J. Arul Hency Sheela, S. Lakshmanan, A. Manikandan, S. Arul Antony, Journal of Inorganic and Organometallic Polymers and Materials 28 (2018) 2388–2398.
3. M. Maria Lumina Sonia, S. Anand, V. Maria Vinosel, M. Asisi Janifer, S. Pauline, A. Manikandan, Journal of Magnetism and Magnetic Materials, 466 (2018) 238-251.
4. A.T. Ravichandran, J. Srinivas, A. Manikandan, A. Baykal, Journal of Superconductivity and Novel Magnetism, 32 (2019) 1663–1670.
5. A.D. Korkmaz, S. Güner; Y. Slimani, H. Gungunes, Md. Amir; A. Manikandan, A. Baykal, Journal of Superconductivity and Novel Magnetism, 32 (2019) 1057–1065.
6. A. Baykal, S. Guner, H. Gungunes, K.M. Batoo, Md. Amir, A. Manikandan, Journal of Inorganic and Organometallic Polymers and Materials, 28 (2018) 2533–2544,
7. Y. Slimani, A. Baykal, Md. Amir, N. Tashkandi, H. Güngüneş, S. Guner, H.S. El Sayed,F. Aldakheel, T.A. Saleh, A. Manikandan, Ceramics International, 44 (2018) 15995-16004
8. Md Amir, H. Gungunes, Y. Slimani, N. Tashkandi, H.S. El Sayed, F. Aldakheel, M. Sertkol, H. Sozeri, A. Manikandan, I. Ercan, A. Baykal, Journal of Superconductivity and Novel Magnetism, 32 (2018) 557–564.
9. A. Manikandan, M. Durka, S. Arul Antony, J. Supercond. Nov. Magn., 28 (2015) 209–218.
10. K. Jeyabanu, P. Devendran, A. Manikandan, R. Packiyaraj, K. Ramesh, N. Nallamuthu, Physica B: Condensed Matter, 573 (2019) 92-101.
11. G. Mathubala, A. Manikandan, S. Arul Antony and P. Ramar, J. Mol. Struct., 1113 (2016) 79-87.
12. A. Manikandan, E. Hema, M. Durka, K. Seevakan, T. Alagesan, S. Arul Antony, J. Supercond. Nov. Magn., 28 (2015) 1783-1795.
13. E. Hema, A. Manikandan, M. Gayathri, M. Durka, S. Arul Antony, B. R. Venkatraman, J. Nanosci. Nanotech. 16 (2016) 5929-5943.
14. M. Maria Lumina Sonia, S. Anand, S. Blessi, S. Pauline, A. Manikandan, Ceramics International, 44 (2018) 22068-22079.
15. A. Manikandan, E. Manikandan, S. Vadivel, M. Kumaravel, D. Maruthamani,S. Hariganesh, Photocatalysis: Present, past and future (Organic Pollutants in Wastewater-I Methods of Analysis, Removal and Treatment), Materials Research Foundations, 29 (2018) 34 Pages, DOI: http://dx.doi.org/10.21741/9781945291630-7
16. G. Padmapriya, A. Manikandan, V. Krishnasamy, S. K. Jaganathan, S. Arul Antony, J. Supercond. Nov. Magn., 29 (2016) 2141-2149.
17. M. A. Almessiere, Y. Slimani, H. Gungunes, A. Manikandan, A. Baykal, Results in Physics, 13, (2019) 102166.
18. A. Manikandan, S. Arul Antony, R. Sridhar, Seeram Ramakrishna, M. Bououdina, J. Nanosci. Nanotech. 15 (2015) 4948-4960.
19. G. Mathubala, A. Manikandan, S. Arul Antony, P. Ramar, Nanosci. Nanotech. Lett. 8 (2016) 375-381.
20. K. Elayakumar, A. Dinesh, A. Manikandan, P. Murugesan, G. Kavitha, S. Prakash, R. Thilak Kumar, S. K. Jaganathan, A. Baykal, Journal of Magnetism and Magnetic Materials, 476 (2019) 157-165.
21. A. Manikandan, M. Durka, S. Arul Antony, Adv. Sci., Eng. Med., 7 (2015) 33-46.
22. E. Hema, A. Manikandan, P. Karthika, M. Durka, S. Arul Antony, B. R. Venkatraman, J. Nanosci. Nanotech. 16 (2016) 7325-7336.
23. A. Manikandan, M. Durka, S. Arul Antony, J. Supercond. Nov. Magn., 28 (2015) 2047–2058.
24. K. Seevakan, A. Manikandan, P. Devendran, Y. Slimani, A. Baykal, T. Alagesan, Journal of Magnetism and Magnetic Materials, 486 (2019) 165254.
25. R. A. Senthil, S. Osman, J. Pan, Y. Sun, T. R. Kumar, A. Manikandan, Ceram. Int. 45 (2019) 18683-18690
26. K. Elayakumar, A. Manikandan, A. Dinesh, K. Thanrasu, K. Kanmani Raja,R. Thilak Kumar, Y. Slimani, S. K. Jaganathan, A. Baykal, Journal of Magnetism and Magnetic Materials, 478 (2019) 140–147.

AUTHORS PROFILE

P. Antony Lyla Msc, MPhil, BEd,Assistant Professor, Department of Physics, Bharath Institute Of Higher Education and Research, Chennai, Tamil Nadu

Dr E. Thirumal M.Sc.,Ph.D, Associate Professor**,** Department of Physics, Faculty of Arts and Science, Bharath Institute Of Higher Education and Research, Chennai, Tamil Nadu

Sahaya Lenin.D, BE, ME, MISTE Assistant Professor, Department of ECE,Hindustan Institute of Technology and Science, Chennai, Tamil Nadu